

Molybdenum-promoted Surface Reconstruction in Polymorphic Cobalt for Initiating Rapid Oxygen Evolution

Juan Bai, Jun Mei,* Ting Liao,* Qiang Sun, Zhi-Gang Chen, Ziqi Sun*

Dr. Juan Bai, Dr. Jun Mei, Prof. Ting Liao, Prof. Ziqi Sun

Centre for Materials Science, Queensland University of Technology, 2 George Street, Brisbane, QLD 4000, Australia.

E-mail: j2.mei@qut.edu.au; t3.liao@qut.edu.au; ziqi.sun@qut.edu.

Dr. Juan Bai, Dr. Jun Mei, Prof. Ziqi Sun

School of Chemistry and Physics, Queensland University of Technology, 2 George Street, Brisbane, QLD 4000, Australia.

Prof. Ting Liao

School of Mechanical Medical and Process Engineering, Queensland University of Technology, 2 George Street, Brisbane, QLD 4000, Australia.

Dr. Qiang Sun

School of Mechanical and Mining Engineering, The University of Queensland, Brisbane, QLD 4072, Australia.

Prof. Zhi-Gang Chen

Centre for Future Materials, University of Southern Queensland, Springfield Central, Brisbane, QLD 4300, Australia.

Prof. Zhi-Gang Chen

School of Mechanical and Mining Engineering, The University of Queensland, Brisbane, QLD 4072, Australia.

Abstract: It has been well recognized that the surface reconstruction of electrocatalysts at the initial stage in the forms of phase transitions, defect migrations, valence regulations, *etc.*, plays critical roles in generating real surficial active catalytic centres and achieving steady surface reactions. It is also expected that a low activation energy barrier for initiating surface reconstruction is crucial for rapid and stable electrochemical catalysis. Despite this, the surface reconstruction kinetics and their effects on catalytic reactions are rarely investigated. Herein, based on phase modulated polymorphic cobalt-based catalysts with tailorable nitrogen-metal bonds through a cationic molybdenum-substitution strategy, real-time X-ray photoelectron spectroscopy (XPS) structural monitoring on the surface chemical state evolutions during the catalytic reaction is performed to track the initial surface reconstruction kinetics during an alkaline oxygen evolution reaction (OER). It is concluded that the molybdenum-modulated cobalt-based nanocatalyst can be tuned with favourable initial surface reconstruction and much stabilized active centres to reach optimized OER catalysis, accompanied by a low onset overpotential of only 210 mV and a favourable overpotential at 10 mA cm⁻² of 290 mV, outperforming the commercially noble-metallic RuO₂ catalyst. This study thus provides new conceptual insights into rationally regulating initial surface reconstruction kinetics for high-performance electrocatalysis reactions.

Keywords: surface reconstruction, electrocatalysts, cobalt, oxygen evolution reaction, molybdenum

1. Introduction

Electrocatalysts for achieving efficient oxygen evolution reaction (OER), a kinetically sluggish half-reaction for water splitting and a rate-controlling step in the overall electrochemical hydrogen production, have been extensively explored to provide efficient hydrogen fuel generation. [1-3] OER is an electrochemical process whose reaction pathway is depending on the pH of the electrolytes. In acidic electrolytes, two water molecules combine to produce four protons and O₂. [4] Oxygen production in alkaline media mainly depends on the oxidation of hydroxide (OH⁻). Compared to acidic OER, OER catalysis in alkaline electrolytes shows more favorable reaction kinetics. In addition, due to the poor activity and stability of the catalyst under acidic conditions, the choice of catalyst is very narrow, mainly relying on noble metal catalysts (Ru-/Ir-based catalysts). [5] In spite of satisfying kinetics and good structural stability of the state-of-the-art ruthenium oxide (IrO₂ and RuO₂) electrocatalyst for OER, the natural scarcity and high costs have greatly hindered its practical application. [6-8] To address the issue, the discovery of alternative catalysts with reduced utilization of noble metals or even without noble metals is a promising solution to reach industrial scale water splitting. [9,10] Among the discovered the earth-abundant and non-noble-metal-containing catalysts, such as oxides, hydroxide, sulfides, phosphides, nitrides, *etc.*, the transition metal oxide-based catalysts have received particular attention in recent years. [11-16] However, during the electrocatalysis procedure, most transition metal-containing catalysts suffer surface reconstruction processes in the forms of phase transformations, defects generations/migrations, valence variations, *etc.* [17] It means that the transition metal-containing catalysts actually are only pre-catalysts and the real active centres only appear after the surface reconstruction processes. [18] From this viewpoint, an energy favourable surface reconstruction process during the initial stage can significantly accelerate the catalytic kinetics and contribute to generate stable active sites, and thus considerably enhancing the OER performance. [19] It has reported that a low activation energy barrier for initiating surface reconstruction is crucial for achieving rapid and stable OER, [20] and the level of dif-

difficulty of the initiation of the surface reconstruction can be read from the onset overpotential of the catalysts, in which a lower onset overpotential means a lower energy barrier for surface reconstruction.^[21] A rapid low-barrier surface reconstruction can achieve rapid creation and stabilization of active centres for following long-time operation, can reduce the whole energy consumption during the electrocatalysis, and enhance the overall reaction stability, which are highly desired for industrial-scale production.

Although surface reconstruction phenomena have been observed in transition metal-containing catalysts during OER, the direct study on the surface reconstruction kinetics at the most initiation stage and then modulating the reconstruction kinetics to enhance the overall catalytic kinetics has been rarely investigated.^[22,23] The well-modulated initial surface reconstructions can reduce the whole energy consumption during electrocatalysis and enhance reaction stability when at a scale-up level, which are highly desired for industrial production. Herein, we choose a typical transition metal oxide catalyst, polymorphic cobalt oxides, as the platform to tune the phase compositions to examine the initial surface reconstruction kinetics and their effects on the OER catalytic activity and performance. Cobalt-containing catalysts, particularly the polymorphic cobalt oxides, have exhibited comparable catalytic activities to these noble metal-based catalysts.^[24-26] In the OER catalysis, most cobalt-containing catalysts work as pre-catalysts and undergo surface reconstruction, such as the phase transition into cobalt oxyhydroxide (CoOOH) and the formation of reversible redox pairs.^[17,27,28] Theoretical calculations have also suggested that the reconstructed surfaces demonstrate higher OER activity than the original surface structures, indicating the important role of the surface reconstruction during the OER catalysis. Unfortunately, no direct investigations on the real-time surface reconstructions occurred on the cobalt-based catalysts and the insights on how the initial surface reconstruction impacts the thereafter OER catalysis yet remains as unclear.

In this work, ultrathin two-dimensional (2D) polymorphic cobalt oxide catalysts consisting of cobalt oxide (CoO), face-centred cubic (*fcc*) metallic cobalt phase, and/or metastable hexagonal close-packed (*hcp*) metallic cobalt phase, are engineered with different initial surface reconstruction kinetics for

OER catalysis. It should be noted that there are two common metallic cobalt polymorphs, i.e., *hcp* and *fcc* phases. The *hcp* phase has higher electron density around the Fermi level, which induces a strong electron coupling over the phase interfaces and can promote various types of catalysis reactions.^[29] The *hcp* phase, however, is metastable, which might be converted into the *fcc* phase at an elevated temperature above 450 °C.^[30,31] At here, by using a cationic molybdenum-substitution strategy, we use molybdenum as substitution atoms to stabilize the catalytically active *hcp* phase after heat treatment. Even though phase engineering of the catalysts with the co-existence of multiple phases has been reported to be an effective approach to improve the catalytic activity, the stabilization of metastable phases yet remains as a challenge. During the synthesis of this work, molybdenum was added as substitution atoms, which will act as two primary functions, namely, stabilizing the metastable metallic *hcp* cobalt phase as an electron-donor and accelerating the surface reconstruction during OER as a kinetic promotor. It has been reported that an effective electron-donor substitution into the 2D nanostructures can form unique surface dipoles, which not only stabilizes metastable surface structure but also gives higher chemical reactivity.^[32,33] Also, it has been evidenced that the high-valence molybdenum sites could act as an intermediate modulator to facilitate the oxidization transition cycles and greatly lower the OER overpotentials in cobalt-based catalysts.^[34-37]

Through monitoring the real-time the surface reconstruction kinetics, it is concluded that the molybdenum-substituted catalysts composed of CoO and metallic *hcp* cobalt phases presents the rapidest surface reconstruction kinetic and the best OER catalysis performance. The onset overpotential of the optimal molybdenum-substituted polymorphic cobalt catalyst is only 210 mV, corresponding to ~20% lower than that of the noble-metallic RuO₂ catalyst for OER. Furthermore, a low overpotential of only 290 mV is required for achieving 10 mA cm⁻² in the alkaline medium and the OER performance can be maintained for 35 h with an negligible overpotential increase. This study, for the first time, reveals the critical role of surface reconstruction kinetics on the electrochemical catalysis and provides insights into the design of high-performance transition metal-based catalysts.

2. Results and discussion

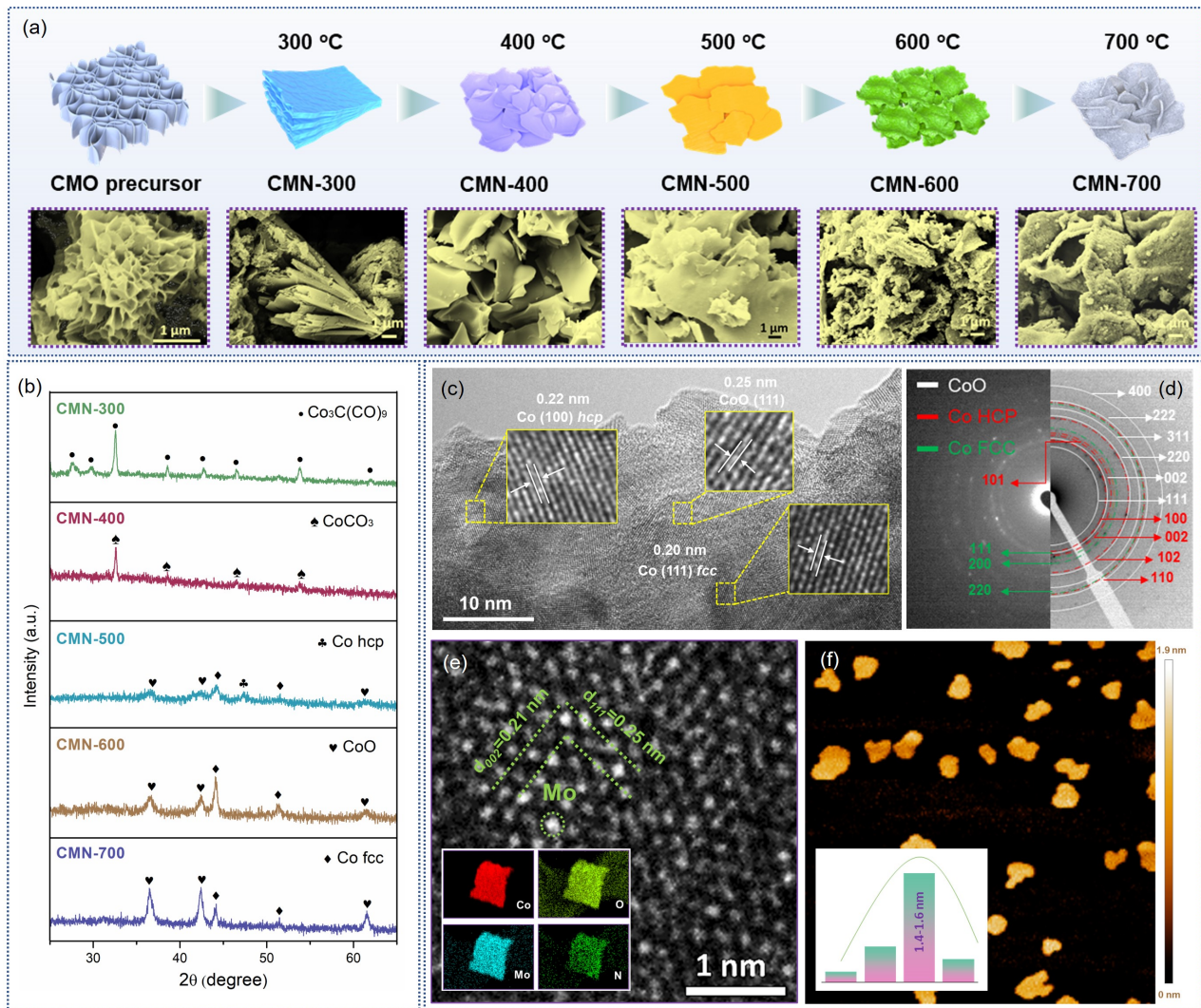


Figure 1. Morphology and phase evolution of molybdenum-substituted polymorphic cobalt catalysts. (a) Morphological evolution of molybdenum-substituted polymorphic cobalt catalysts (CMN- X , $X = 300$ – 700 °C). (b) Phase evolution of molybdenum-substituted polymorphic cobalt catalysts examined by X-ray diffraction (XRD). (c) High-resolution transmission electron microscopy (HR-TEM) and (d) selected area electron diffraction (SAED) identification of the CMN-500 catalyst, confirming the co-existence of CoO and metallic Co (*hcp* and *fcc*) phases. (e) Aberration-corrected cold field emission transmission electron microscopy (Cs-STEM/TEM) image of the CMN-500 catalyst showing the presence of molybdenum atoms in polymorphic cobalt structure. Inset in *e* shows the element mappings patterns of the CMN-500 catalyst. (f) Atomic force microscopy (AFM) image of the assembled polymorphic cobalt in the CMN-500 catalyst.

To examine the initial surface reconstruction kinetics of the catalysts, typical polymorphic cobalt-based 2D nanosheets with proper phase engineering of consist of different phases of CoO, *fcc* metallic cobalt phases, and/or *hcp* metallic cobalt phase to provide different potential-dependant surface reconstruction kinetics were synthesized by a surfactant-assisted self-assembly approach. Specifically, the molybdenum-substituted 2D cobalt hydroxide nanosheets (denoted as CMO precursor) was synthesized from the surfactant-stabilizing solution containing Pluronic P123 and ethylene glycol (EG).^[38] To achieve the conversion of the precursor nanosheets into the desired phase compositions, a following urea reduction of the CMO in an argon flow was performed at temperatures ranging from 300 to 700 °C, and the corresponding samples were denoted as CMN-*X* (*X* is the annealing temperature, 300-700 °C). The morphology of the CMN-*X* samples was examined by scanning electron microscopy (SEM). As illustrated in **Figure 1a**, it is interesting that the 2D morphology could be well maintained up to 500 °C. When the annealing temperatures were above 500 °C, the 2D morphology was lost resulted by possible agglomeration and sintering.

Figure 1b presents the phase evolution of the 2D nanostructures. When the temperature was lower than 400 °C, cobalt carbonates, $\text{Co}_2\text{C}(\text{CO})_9$ in the CMN-300 and CoCO_3 in the CMN-400, were detected, resulted by the reaction between the cobalt-containing phases and the residual small molecules. At 500 °C, two types of metallic cobalt phases, i.e., *hcp* phase (PDF No. 05-0727) and *fcc* phase (PDF No. 15-0806), were clearly identified and co-existed with a CoO phase. Further temperature increasing to 600 °C or above, the *hcp* cobalt phase disappeared and only the *fcc* cobalt phase and the CoO phase were found. To clarify the role of molybdenum substitution as a phase stabilizer, the reference sample was synthesized without the addition of molybdenum at 500 °C, in which only the *fcc* cobalt phase was obtained (denoted as Co-U, **Figure S1**). Notably, a reduction atmosphere is also very critical for the formation of metallic phase. Without the addition of urea, only molybdenum-doped CoO was obtained (CMO, **Figure S2**). It should be stressed that the introduced nitrogen in polymorphic cobalt catalyst,

which was originated from solid urea under thermal reduction, could narrow the bandgap and optimize the OH⁻ cleavage for promoting OER.^[39-41]

The phase composition and the existence of molybdenum were further confirmed by the transmission electron microscopes (TEM). As shown in the high-resolution TEM (HRTEM) image in **Figure 1c**, three types of phases were identified in the CMN-500 sample, which are CoO exposed with the (111) facets, the *fcc* cobalt phase with the (111) planes, and the *hcp* cobalt phase with the (100) planes. The selected-area electron diffraction (SAED) patterns (**Figure 1d**) for the CMN-500 sample further evidenced the co-presence of CoO, *hcp*, and *fcc* cobalt phases. Energy-dispersive X-ray (EDX) mapping (inset in **Figure 1d**) indicated that the CMN-500 nanosheet was composed of homogeneously distributed elements of Co, Mo, O, and N, where the nitrogen was originated from the reduction of solid urea. High-angle annular dark-field scanning TEM (HAADF-STEM) image coupled with EDX mapping patterns (**Figure S3 and S4**) demonstrates the uniform distribution of cobalt species on the 2D CoO nanosheet and the aberration-corrected transmission electron microscopy (Cs-STEM/TEM) images (**Figure 1e and S5**) confirm the substitution position of the embedded Mo atoms in the CMN-500 sample. It is interesting that a high temperature of 500 °C did not significantly affect the thickness of the 2D nanosheets compared to the CMO precursor. As confirmed by the atomic force microscopy (AFM) characterization, a dominate thickness distribution of the 2D nanosheets was in 1.4-1.6 nm (**Figure 1f and S6**).

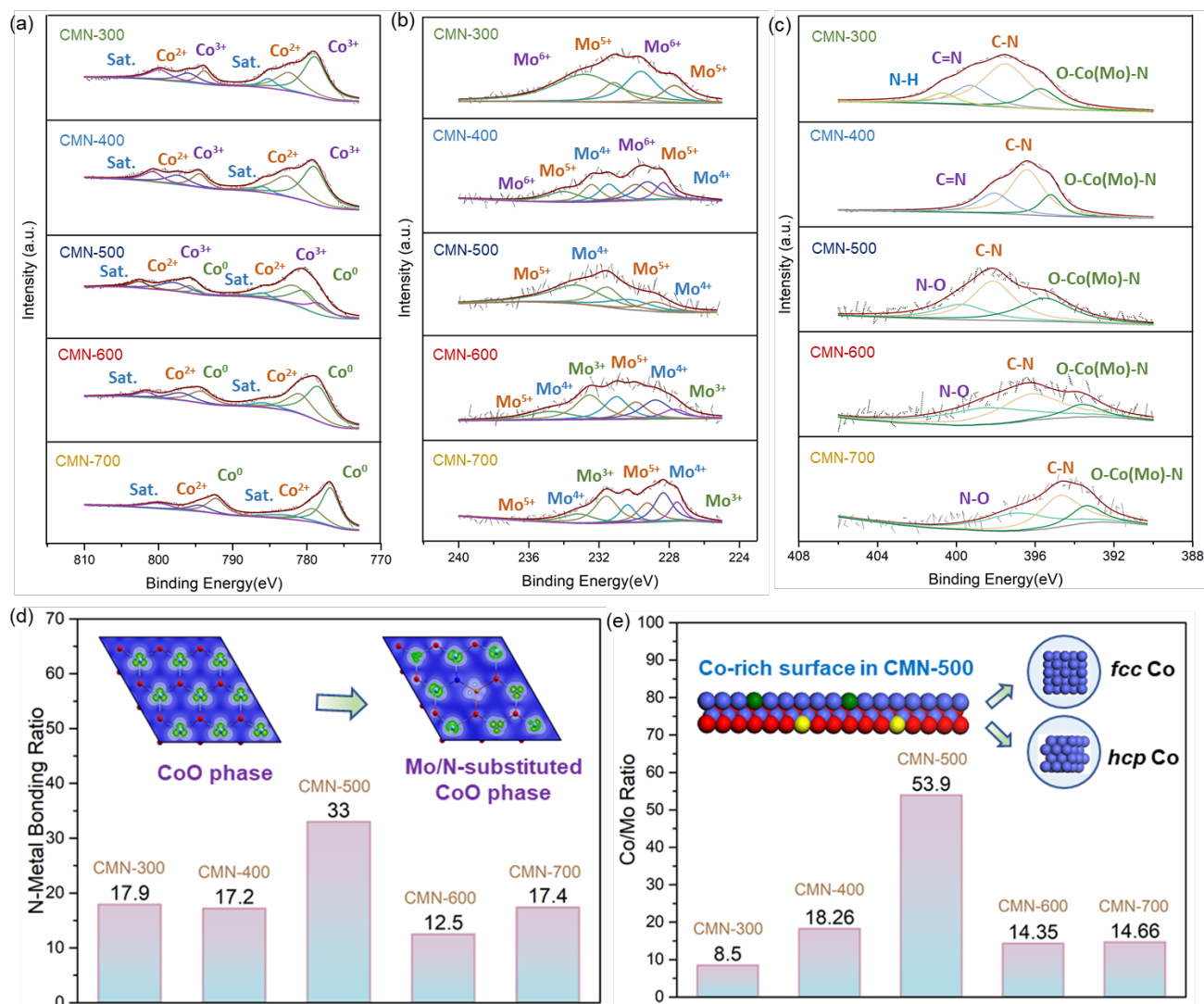


Figure 2. (a-c) High-resolution XPS spectra of (a) Co 2p, (b) Mo 3d, (c) N 1s in the CMN-300, CMN-400, CMN-500, CMN-600 and CMN-700 catalysts. (d) Comparison on the ratio of Co, Mo, and O-Co(Mo)-N based on XPS analysis. Inset in d shows the calculated electron density slice from the Fermi energy range after the incorporation of molybdenum and nitrogen into the cubic CoO phase. (e) Comparison on the Co/Mo ratio in the CMN-X catalysts. Inset in e shows the Co-rich surfaces in the CMN-500 catalyst.

Surface chemical states are sensitive to synthetic conditions and crucial in surface reconstruction processes towards rapid and stable OER. To confirm the individual chemical states of the metallic cobalt, the molybdenum regulating atoms, and the existing nitrogen introduced from the solid urea on the 2D polymeric cobalt nanosheets, X-ray photoelectron spectroscopy (XPS) was applied for examining the specific core levels of Co 2p, Mo 3d, and N 1s of the CMN-X catalysts. From the XPS survey spectra, the relative percentages of the nitrogen and molybdenum species were higher at the temperatures

below 500 °C, but presented a sharp decrease when the temperature was over 500 °C (**Figure S7**). This is largely due to the decomposition of nitrogen-containing organic molecules occurred at 500 °C and the preferred migration of cobalt atoms or favourable formation of cobalt phase to the surface at high temperatures. As to the high-resolution core levels for each element, the obvious position inflection was observed as the temperature varied. Taking the CMN-500 catalyst as a specific example, the two dominant peaks in the Co 2p spectra corresponding to the spin splitting into Co 2p_{3/2} and 2p_{1/2} were identified (**Figure 2a**). The deconvolutions of the main peak pairs at 778.1/794.8, 780.4/795.8, and 781.8/798.2 eV, respectively, were assigned to Co⁰, Co³⁺, and Co²⁺, which clearly exhibited the evolution into metallic cobalt phases on the CoO nanosheets when the temperature reached or beyond 500 °C. For the Mo 3d spectrum, there was also an obvious transition occurred at 500 °C, during which the molybdenum changed from the high valent Mo⁶⁺ and Mo⁵⁺ species to the more reduced Mo⁴⁺ and Mo³⁺ states (**Figure 2b**). According to the XPS results, the overall valence states of Co and Mo tend to shift to relatively low energies, associating with the reduction and the formation of metallic Co⁰ phases above 500 °C (**Table S1 and S2**). Together with the XRD and TEM analysis mentioned above, it could be concluded that 2D polymorphic cobalt catalyst, CMN-500, consisting of the CoO phase, the *fcc* cobalt phase, and the molybdenum-stabilized *hcp* cobalt phase, accompanied by the enriched metal-nitrogen bonds, was successfully obtained with the presence of molybdenum-containing salt precursor and the reduction urea atmosphere reagent at a temperature of 500 °C.

For the N 1s spectra, the nitrogen peak can be mainly divided into N-O, C-N, and O-Co(Mo)-N bindings (**Figure 2c**). A certain negative shift occurred for O-Co(Mo)-N bonds at different temperatures. It is obviously that the surfaces of the CMN-300 and CMN-400 catalysts were dominated by the adsorption of the organic nitrogen-containing species (*e.g.* N-H, C-N, and C=N) associated with the thermal decomposition of the solid urea. As the temperature increased, the surface-nitrogen content decreased significantly with a gradual transition into strong N-Metal bonding at elevated temperatures. Particularly, for the CMN-500 catalyst, the N-Metal bond ratio reached the maximum value of 33 % (**Figure 2d**).

This high amount of surface N-Metal bonds will pose strong influences onto the electronic structure. As shown in the inset in **Figure 2d**, the calculated electron density slice at the Fermi energy confirmed the re-distribution of electron density with the incorporation of molybdenum and nitrogen into the cubic CoO phase, where the electron-depletion molybdenum sites and the electronic rich nitrogen sites significantly affected the surrounding cobalt sites.

We also noted that the surface Co/Mo ratios varied significantly with the heat-treatment temperatures. **Figure 2e** presents the Co/Mo ratio in different catalysts. For the CMN-500 catalyst, the highest ratio of 53.9 for Co/Mo was identified. In conjunction with both the XRD and the TEM results, we can surmise that the formation of *hcp* and *fcc* metallic cobalt phases associated with the migrations of cobalt atoms to the surface, which are reflected by the highest surface Co/Mo ratio at 500 °C. These results thus confirmed that the CMN-500 catalyst delivered the maximum exposed cobalt atoms on the surface, as illustrated in the model presented in the inset in **Figure 2e**. It is expected that the combination of dual-phase metallic cobalt phases and the oxide phase in the CMN-500 catalyst can result in abundant active cobalt sites for rapid surface reconstruction to initiate OER and meanwhile promote the catalytic activity and stability.

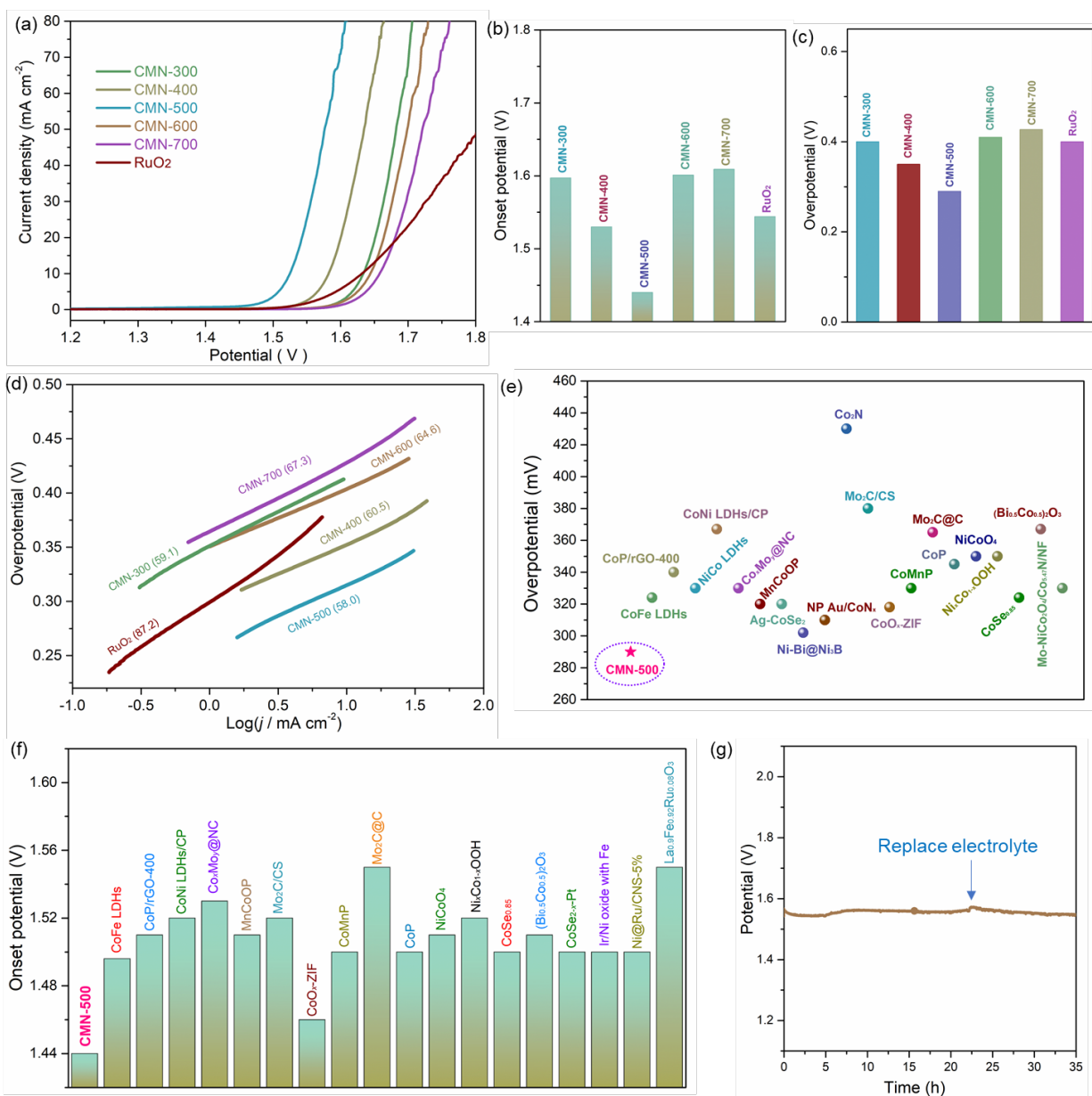


Figure 3. (a) LSV curves of the CMN-*X* catalysts and the commercialized RuO₂ catalyst for OER in an N₂-saturated 1 M KOH solution at the scan rate of 5 mV s⁻¹. (b, c) Comparison on (b) onset potentials and (c) overpotentials at the current density of 10 mA cm⁻². (d) Tafel plots and the corresponding slopes of the CMN-*X* and the commercialized RuO₂ catalysts. (e) Comparison of overpotentials at 10 mA cm⁻² for the CMN-500 catalyst with these reported Co/Mo-based and other transition metal catalysts. (f) Comparison on the onset potentials for the CMN-500 catalyst with these reported catalysts for OER. (g) Chronoamperometric curves of the CMN-500 catalyst for 35 h in alkaline solution.

The OER performances of the CMN-*X* catalysts were investigated in 1M KOH solution. The linear sweep voltammetry (LSV) curves were recorded with a 95% iR-compensation, as presented in **Figure 3a**. To initiate alkaline OER, the CMN-500 catalyst required the lowest onset OER potential of only

1.44 V, much superior to other CMN-*X* catalysts (*e.g.* 1.59 V for the CMN-300 catalyst, 1.53 V for the CMN-400 catalyst, and 1.60 V for the CMN-600 and CMN-700 catalysts) (**Figure 3b**). There was a volcano-like correlation between the catalyst treated in different temperatures and the overpotential for achieving the current density of 10 mA cm⁻². Only 290 mV was required for the CMN-500 catalyst to achieve 10 mA cm⁻², which is much smaller than that for CMN-300 (400 mV), CMN-400 (350 mV), CMN-600 (410 mV), CMN-700 (427 mV), and the commercial RuO₂ catalyst (400 mV) (**Figure 3c**). From the point of view of OER kinetics evaluated by Tafel plots, the CMN-500 catalyst presented the lowest slope value of 58.0 mV dec⁻¹, outperforming the CMN-300 catalyst (59.1 mV dec⁻¹), the CMN-400 catalyst (60.5 mV dec⁻¹), the CMN-600 catalyst (64.6 mV dec⁻¹), the CMN-700 catalyst (67.3 mV dec⁻¹), and the RuO₂ catalyst (87.2 mV dec⁻¹), which implied the superior reaction kinetic for the CMN-500 catalyst (**Figure 3d**). To evaluate the performance levels of the molybdenum-substituted polymorphic cobalt catalyst, the OER performance of the CMN-500 catalyst was compared with some reported transition metal-based OER catalysts, particularly these Co/Mo-containing ones. As shown in **Figure 3e and 3f**, the CMN-500 catalyst delivered the lowest overpotential to reach the same current density of 10 mA cm⁻² and the lowest onset potential, which was much superior to these previously reported OER catalysts, particularly for the dominantly recognized CoFe LDHs (324 mV for the overpotential at 10 mA cm⁻² and 1.496 V for the onset potential) (**Table S3 and S4**).^[42] Besides, the stability is another crucial parameter for the evaluation of electrocatalysts. We examined the potential fluctuation of the CMN-500 catalyst at 10 mA cm⁻², as shown in **Figure 3g**, suggesting no obvious overpotential increase for 35 h, verifying its outstanding durability in the alkaline solution. Moreover, the required overpotentials for achieving high current densities (20 and 50 mA cm⁻²) of the CMN-*X* catalysts were also compared with the RuO₂ reference electrode. It is concluded that the CMN-500 catalyst delivered the smallest overpotentials of 310 and 340 mV at 20 and 50 mA cm⁻², respectively (**Figure S8**).

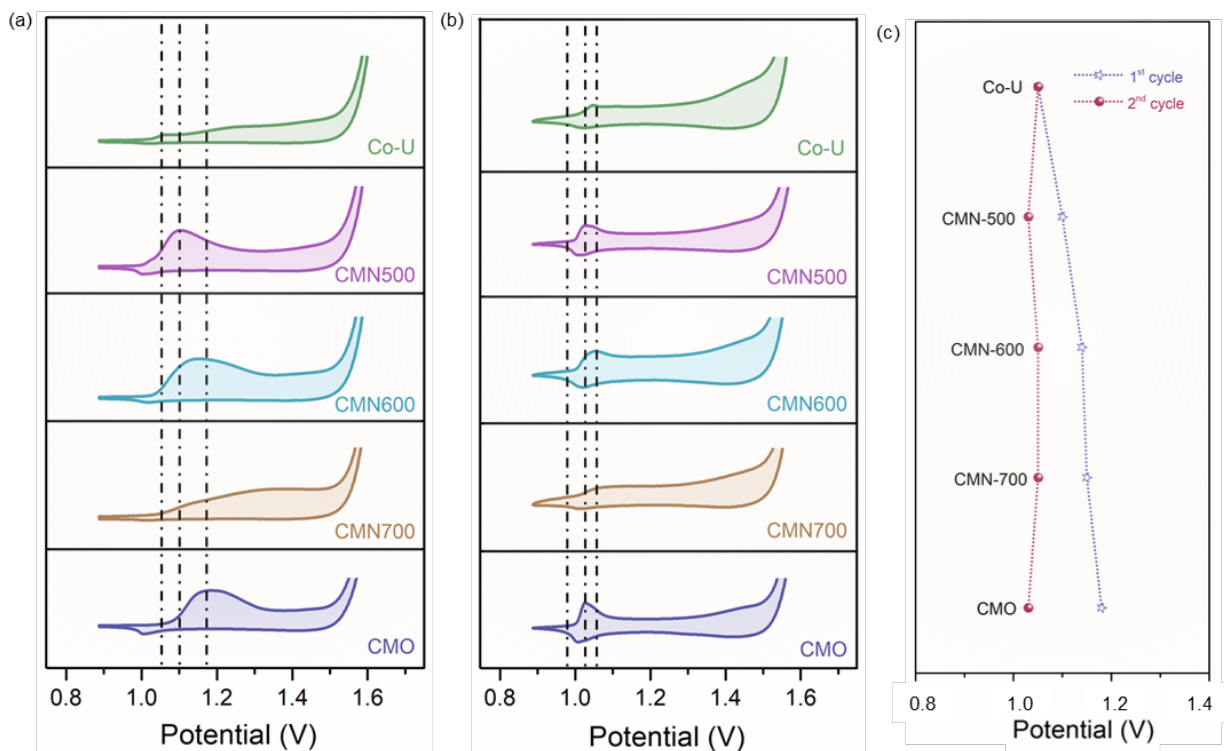


Figure 4. (a) Comparison on the first cyclic voltammetry (CV) cycle and (b) the second CV cycle of the Co-U, CMN-500, CMN-600, CMN-700 and CMO catalysts for alkaline OER. (c) Correlation between redox potential gap and phase composition in the first and second cycles.

The onset potential of electrocatalysis is closely associated with the energy to overcome site blocking to initiate the catalytic reaction and the availability of free active sites.^[43] Electrocatalysis mainly occurs on the surfaces, and the ideal surfaces with exposed active sites are required for initiating reactions. However, for most transition metal-containing catalysts, they often act the roles as pre-catalysts in the practical electrolysis, which means that surface reconstruction is essential for creating real active sites. The onset potential is the lowest energy barrier in responsible to trigger the surface electrochemical reactions. For a pre-catalyst, the onset potential thus should be corresponding to the surface reconstruction reaction prior to the real OER catalytic reactions. As a consequence, a much favorable surface reconstruction kinetic indicates a much lower reconstruction energy barrier and thus a lower onset overpotential at the reaction initiation stage. The lowest onset overpotential of CMN-500 indicates that this catalyst has the rapidest surface reconstruction kinetics and lowest activation energy barrier among the examined catalysts. In order to explore the effects of surface reconstruction on the catalytic

performance for OER and meanwhile identify the crucial role of molybdenum as a reconstruction promotor during the pre-oxidization process, the comparative cyclic voltammetry (CV) cycles were first carried out to examine of the surface redox reactions accompanying with the reconstruction.^[44] As demonstrated in the first CV cycle presented in **Figure 4a**, the oxidation and reduction peaks at the potential below 1.3 V should be attribute to the reversible transformation between Co^{2+} and Co^{3+} .^[45] Generally, the further transition of $\text{Co}^{3+}/\text{Co}^{4+}$ redox couple often occur at about 1.4 V for cobalt-containing catalysts.^[46] For the CMN-500 catalyst with a mixture of $\text{Co}^0/\text{Co}^{2+}/\text{Co}^{3+}$ and abundant exposed surface cobalt sites, the primary pre-oxidation occurred at a wide region of 1.0-1.3 V, corresponding to the formation of cobalt oxyhydroxide (CoOOH).^[47] By a comparison with the CMN-600 catalyst, the pre-oxidization centre potential of the CMN-500 catalyst is much lower, suggesting that the presence of metastable *hcp* cobalt phase stabilized by molybdenum could effectively promote the surface reconstruction reactions. For CMN-700, in which the dominant phases are CoO and *fcc* Co and the Co^0 ratio on the surfaces also significantly increased, only a pre-oxidization potential over 1.4 V was identified. For the Co-U with only the *fcc* cobalt phase and without any additional N-Metal bond, the absence of obvious oxidization peaks indicates that the pre-oxidization at the most initial stage is very difficult on its surfaces, leading to a large activate energy barrier for achieving desired surface reconstruction. For the CMO catalyst, as identified the redox peak and the obvious current densities, the transformations from low-valence $\text{Co}^{2+}/\text{Co}^{3+}$ to high-valence $\text{Co}^{3+}/\text{Co}^{4+}$ were apparent, however, the reduction reaction mainly occurred within the $\text{Co}^{2+}/\text{Co}^{3+}$ redox couple. This relatively large potential gap accompanied by irreversible reconstruction resulted in high energy consumption. Hence, these are not desired for promoting OER, as verified by the larger onset potentials for the Co-U and CMO catalysts (> 1.5 V) compared to the CMN-500 catalyst. Moreover, at the current density of 10 mA cm^{-2} , the overpotentials for the CMO (330 mV) and Co-U (350 mV) catalysts were much larger than that of the CMN-500 catalyst (290 mV) (**Figure S9**). Besides, based on the electrochemical impedance spectroscopy (EIS) analysis, the charge transfer resistance (R_{ct}) of the CMN-500 catalyst is 0.47Ω ,

which is much lower than the CMO (0.97 Ω) and the Co-U (0.70 Ω) catalysts, indicating the best reaction kinetic for alkaline OER (**Figure S10**). Via the electrochemical active surface area (ECSA) comparison for the CMN-500, CMN-600 and CMN-700 catalysts (**Figure S11**), the CMN-500 catalyst delivers the largest specific capacitance of 30.8 mF cm⁻² (CMN-600 (5.99 mF cm⁻² for CMN-600 and 1.79 mF cm⁻² for CMN-700), suggesting the largest expose area.

It should be noted that the differences of both the onset potentials and the major redox potentials only happened in the first cycle. In the subsequent CV cycles, all catalysts showed similar CV behaviours with a reversible redox potential at 1.03-1.05 V (**Figure 4b**), indicating that the real active sites after surface reconstruction are pretty similar and the redox pairs on the surfaces thereafter should be Co²⁺/Co³⁺ for the alkaline OER. **Figure 4c and S12** present the pre-oxidization potential variations for the first two cycles. A very large potential gap accompanied by irreversible reconstruction were observed for CMO catalyst (**Figure 4c**), which resulted in very high energy consumption and can lead to sluggish surface reconstruction kinetics. For the CMN-500, the potential gap between the first two cycles was very small, suggesting the low energy barrier of the surface reconstruction. For the Co-U with dominant *fcc* cobalt phase, an unobvious change on the oxidation potential was observed but the onset potential was large, implying that the favourable surface reconstruction was not achieved in the first two cycles. In the subsequent CV cycles, all catalysts showed similar CV behaviours with a reversible redox potential at 1.03-1.05 V (**Figure 4b**), indicating that the real active sites after surface reconstruction are pretty similar and the redox pairs on the surfaces thereafter should be Co²⁺/Co³⁺ for the alkaline OER. Based on the above results, the CMN-500 catalyst exhibited a much favourably surface reconstruction with a small oxidization potential change over cycles, which verified that the co-existence of the mixed metallic cobalt (*hcp* and *fcc*) and the CoO phases can facilitate the initial surface reconstruction processes during the alkaline OER, reach the reversible redox transitions, and thus promote the catalytic reaction activity.

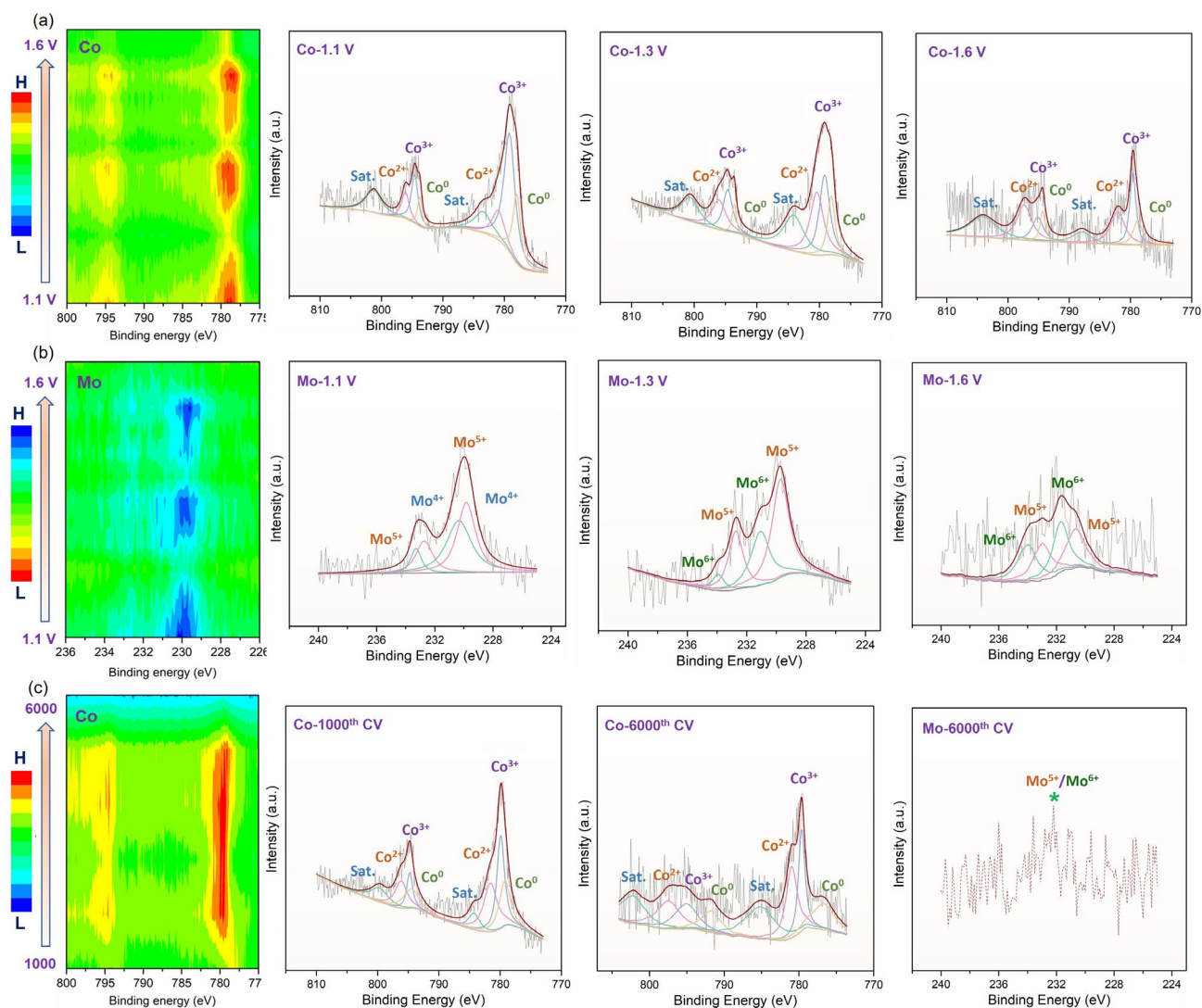


Figure 5. (a, b) Potential-dependent XPS structural evolution of (a) Co 2p and (b) Mo 3d in the CMN-500 catalyst at the reconstruction stage within the potential ranging from 1.1 to 1.6 V during the alkaline OER, and the corresponding fitted XPS spectra at the potential of 1.1 V, 1.3 V and 1.6 V. (c) Structural evolution of cobalt species during 6000 CV cycles during the alkaline OER, and the fitted XPS spectra of Co 2p after 1000 and 6000 CV cycles, and high-resolution XPS spectrum of Mo 3d after 6000 CV cycles.

To further explore the roles of cobalt, molybdenum, and nitrogen during the surface reconstruction, the potential-dependent structural changes on the CMN-500 catalyst surface were tracked by using the XPS technique. As demonstrated in **Figure 5a** for cobalt and **Figure 5b** for molybdenum, the surface states were examined in the potential range from 1.1 to 1.6 V during OER. As the potential increased, the region located at low energies became relatively narrow, indicating the gradual oxidization process-

es of both cobalt and molybdenum in the CMN-500 catalyst. Specifically, for Co 2p, the dominate peaks attributed to Co^{3+} became more sharp, suggesting the appearance of CoOOH during surface reconstruction and meanwhile confirming the Co^{3+} as the real active sites for OER.^[48,49] Similar intensity variations and positive shifting were also observed for molybdenum, as shown in **Figure 5b**, indicating the oxidation into Mo^{5+} and Mo^{6+} with the highest valence with the increase of voltages. Furthermore, the surface chemical state variations of both the cobalt and the molybdenum during the long-term CV cycling up to 6000 cycles were tracked to confirm the stability after surface reconstruction. As demonstrated in **Figure 5c**, no obvious further structural evolution for Co^{3+} was observed during the 6000 CV cycles towards OER, which confirms the highly reversible redox transitions and the stable catalytic activity of the real active sites created during surface reconstruction in the CMN-500 catalyst. Based on these added TEM results (**Figure S13 and S14**), it can be concluded that the morphology remains unchanged, accompanied by the loss of molybdenum and the formation of Co(III)OOH after 6000 CV cycles, which are well consistence with the XPS results. On the contrary, the chemical coordination of molybdenum became complicated as the cycles increased, evidenced by inapparent XPS peaks located at high-energy regions, which might be resulted by relocation of molybdenum into the catalysts to stabilize the reconstructed surface structures. By taking samples from the solutions after 6000 CV cycles for ICP-MS test, the concentration of molybdenum was 1.31 ppm (the average value for three-time tests by using the Agilent 8800 Inductively Coupled Plasma Mass Spectrometer (ICP-MS) equipment), indicating the dissolution of molybdenum during CVs. These results conclude that the dislocation and oxidization of molybdenum is much favourable for creating active defective sites and thus promoting surface reconstruction kinetics in contact with water molecules, and the reconstruction of cobalt is crucial for sustaining stable OER performance. As demonstrated by **Figure S15 and S16**, the metastable hcp phase is fully converted into the active Co(III)OOH active species after both CV cycles and long-time stability tests. However, the fcc phase remained as unchanged. This further verify the Mo-stabilized hcp phase has much favorable surface reconstruction kinetic and can be much easier con-

verted into OER active Co(III). XPS analysis also confirm the similar changes on valence states of Co, Mo, and N species to these after CV cycles (**Figure S17**).

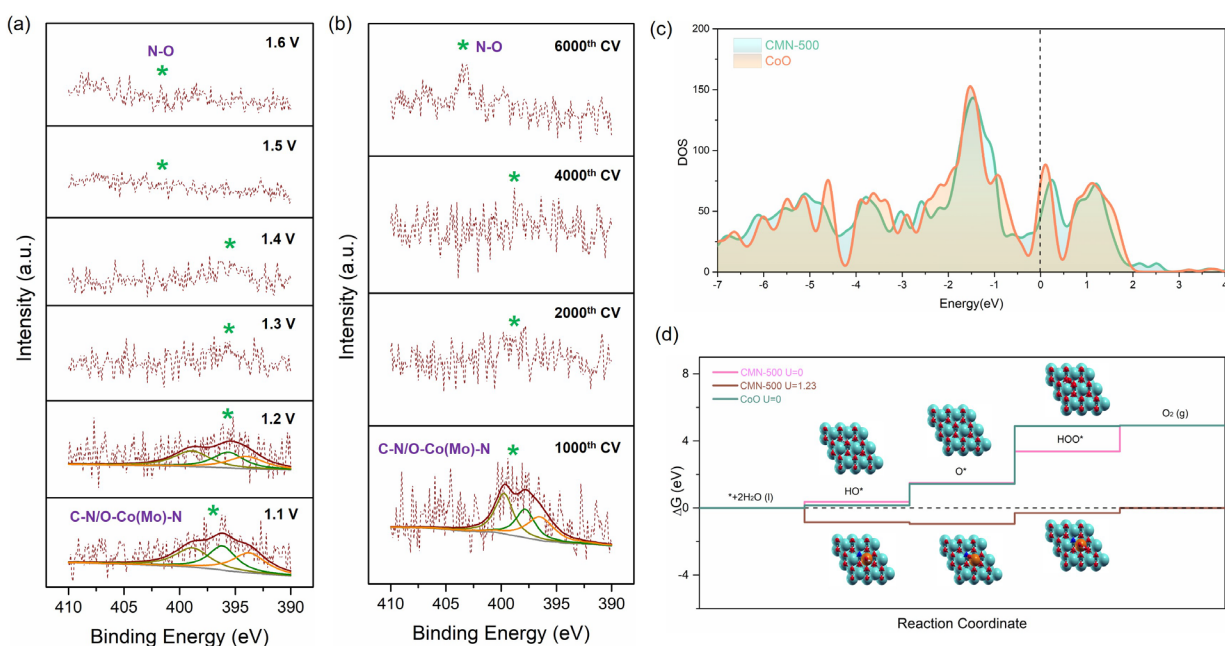


Figure 6. (a, b) *Ex situ* XPS structural evolution of nitrogen at the potential between 1.0 V and 1.6 V, and at different CV cycles ranging from 1000 to 6000 during the alkaline OER. (c) Calculated density of states (DOS) and (d) the free energy steps of the CMN-500 catalysts and the reference CoO surface for OER.

The roles of nitrogen in surface reconstruction stage were uncovered via a combination of XPS characterization and theoretical calculations. As compared in **Figure 6a**, as the potential increased, a positive energy shift was identified, accompanied by the detachment and oxidation of nitrogen from N-Metal bonds. After maximum 6000 CV cycles, an obvious peak located at around 403 eV attributed to oxidized nitrogen (N-O) was detected (**Figure 6b**),^[50,51] verifying that the loss of nitrogen was caused by the reconstruction as the OER proceeds. It is inferred that nitrogen species were detached from the crystal lattices during surface reconstruction processes to produce a defective environment and the reaction intermediates easily moved towards defective sites accompanied by the formation of form CoOOH.^[21,52] To better uncover the specific roles of N-Metal bonding for OER, density functional

theory (DFT) calculations were performed. First, the calculated density of states (DOS) confirmed the metallic characteristic of the ultrathin 2D CoO nanosheets with the presence of N-Metal bonds (**Figure 6c**).^[53–55] Then, the Gibbs free energy profile of the OER intermediates was calculated, as compared in **Figure 6d**, without the application of an external potential ($U = 0$ V), the adsorption of the HOO* intermediate on the reference CoO catalyst is the rate-determining step (RDS) with the largest free energy barrier of 3.45 eV. After the introduction of N-Metal bonds and molybdenum sites, the free energy of the RDS significantly decreased into 1.88 eV, suggesting that the Co(Mo)-N bonds are beneficial to optimizing the intermediate adsorption during OER and thus lowering the OER overpotential. If an external potential of 1.23 V applied, the whole reaction can be readily proceeded. From this viewpoint, the N-Metal bonds in the CMN-500 catalyst are also critical in initiating the surface reconstruction and to enhance the OER catalysis with much favourable energy consumption.

On the whole, the resultant CMN-500 catalysts delivered a much favourable surface reconstruction kinetics for achieving rapid and stable OER, as evidenced by the lowest onset overpotential and the lowest overpotential at 10 mA cm^{-1} . By structural tracking characterizations, the underlying promotion mechanism was revealed and summarized as follows: (i) molybdenum is crucial for stabilizing the metastable *hcp* metallic phase during the catalyst preparation stage, and meanwhile stabilizing the real active sites (Co^{3+}) at the surface reconstruction stage; (ii) the migration and/or detachment of cationic molybdenum and anionic nitrogen is much favourable for creating defective environment and promoting highly active surfaces; (iii) the presence of nitrogen for N-Metal bonding is beneficial to modulating the reaction intermediation adsorption, particularly at the reaction initiation stage. Hence, the desired surface reconstruction could be easily achieved with the assistance of the molybdenum promotor in polymeric cobalt catalysts.

3. Conclusions

In summary, phase engineered molybdenum-substituted 2D polymorphic cobalt-based catalysts were fabricated to examine the surface structural reconstruction at the initial stage and its effect on achieving rapid and stable OER catalysis. By tracking the initial surface reconstruction during alkaline OER via both in-situ and ex-situ XPS technique, the surface reconstruction kinetics during the OER were monitored. It is concluded that the presence of metastable metallic *hcp* cobalt co-existing with the N-Metal bonds allows rapid surface reconstruction from the multiple states into the real and stable reaction sites of $\text{Co}^{3+}/\text{Co}^{2+}$ redox couples. As a result, the regulated polymorphic cobalt catalyst delivers an onset potential as low as 1.44 V and a low overpotential of 290 mV at 10 mA cm^{-2} in the alkaline media. This study provides new conceptual insights on rationally regulating the initial surface reconstruction kinetics and offers some insights into the catalytic mechanisms of the OER catalysis.

Supporting Information

Supporting Information is available from the Wiley Online Library or from the author.

Acknowledgement

This work was supported by an ARC Discovery Project (DP200103568) and two ARC Future Fellowship projects (FT180100387 and FT160100281). J. Mei acknowledges the financial support by the QUT ECR Scheme Grant (No. 2020001179). The authors thank Central Analytical Research Facility (CARF) and the grants of CPU time from the Australian National Computational Infrastructure Facility and the High-performance Computing Centre of QUT. The authors thank Dr Osama Yousef Ali Ghidan (Sam), Dr Sunny Hu, and Mr. Tal Cooper for kindly help on the ICP tests.

Received: ((will be filled in by the editorial staff))

Revised: ((will be filled in by the editorial staff))

Published online: ((will be filled in by the editorial staff))

References

- [1] H. Mistry, A. S. Varela, S. Köhl, P. Strasser, B. R. Cuenya, *Nat. Rev. Mater.* **2016**, *1*, 16009.
- [2] Z. W. Seh, J. Kibsgaard, C. F. Dickens, I. Chorkendorff, J. K. Nørskov, T. F. Jaramillo, *Science* **2017**, *355*, eaad4998.
- [3] J. Mei, T. He, J. Bai, D. Qi, A. Du, T. Liao, G. A. Ayoko, Y. Yamauchi, L. Sun, Z. Sun, *Adv. Mater.* **2021**, 2104638.
- [4] J. Gao, H. Tao, B. Liu, *Adv. Mater.* **2021**, *33*, 1.
- [5] L. Li, P. Wang, Q. Shao, X. Huang, *Adv. Mater.* **2021**, 2004243, 1.
- [6] Q. Shi, C. Zhu, D. Du, Y. Lin, *Chem. Soc. Rev.* **2019**, *48*, 3181.
- [7] M. Luo, Y. Yang, Y. Sun, Y. Qin, C. Li, Y. Li, M. Li, S. Zhang, D. Su, S. Guo, *Mater. Today* **2019**, *23*, 45.
- [8] D. Y. Chung, P. P. Lopes, P. Farinazzo Bergamo Dias Martins, H. He, T. Kawaguchi, P. Zapol, H. You, D. Tripkovic, D. Strmcnik, Y. Zhu, S. Seifert, S. Lee, V. R. Stamenkovic, N. M. Markovic, *Nat. Energy* **2020**, *5*, 222.
- [9] J. Mei, T. Liao, J. Liang, Y. Qiao, S. X. Dou, Z. Sun, *Adv. Energy Mater.* **2020**, *10*, 1901997.
- [10] J. Mei, J. Bai, G. A. Ayoko, H. Peng, T. Liao, Z. Sun, *Adv. Energy Sustain. Res.* **2021**, *2*, 2100057.
- [11] L. An, C. Wei, M. Lu, H. Liu, Y. Chen, G. G. Scherer, A. C. Fisher, P. Xi, Z. J. Xu, C. H. Yan, *Adv. Mater.* **2021**, *33*, 2006328.
- [12] X. Liu, L. Dai, *Nat. Rev. Mater.* **2016**, *1*, 16064.
- [13] Z. P. Wu, X. F. Lu, S. Q. Zang, X. W. Lou, *Adv. Funct. Mater.* **2020**, *30*, 1910274.
- [14] Z. Xu, Y. Ying, G. Zhang, K. Li, Y. Liu, N. Fu, X. Guo, F. Yu, H. Huang, *J. Mater. Chem. A* **2020**, *8*, 26130.
- [15] Y. Huang, S. L. Zhang, X. F. Lu, Z. P. Wu, D. Luan, X. W. Lou, *Angew. Chemie - Int. Ed.* **2021**, *60*, 11841.
- [16] Z. P. Wu, H. Zhang, S. Zuo, Y. Wang, S. L. Zhang, J. Zhang, S. Q. Zang, X. W. Lou, *Adv. Mater.* **2021**, *33*, 2103004.
- [17] X. Liu, J. Meng, J. Zhu, M. Huang, B. Wen, R. Guo, L. Mai, *Adv. Mater.* **2021**, *33*, 2007344.
- [18] H. Ding, H. Liu, W. Chu, C. Wu, Y. Xie, *Chem. Rev.* **2021**, *0*, 10.1021/acs.chemrev.1c00234.
- [19] Y. Pi, Y. Xu, L. Li, T. Sun, B. Huang, L. Bu, Y. Ma, Z. Hu, C. W. Pao, X. Huang, *Adv. Funct. Mater.* **2020**, *30*, 2004375.
- [20] L. Gao, X. Cui, C. D. Sewell, J. Li, Z. Lin, *Chem. Soc. Rev.* **2021**, *50*, 8428.
- [21] A. Sivanantham, P. Ganesan, A. Vinu, S. Shanmugam, *ACS Catal.* **2020**, *10*, 463.
- [22] Y. Li, X. Du, J. Huang, C. Wu, Y. Sun, G. Zou, C. Yang, J. Xiong, *Small* **2019**, *15*, 1901980.
- [23] Y. Wu, J. Yang, T. Tu, W. Li, P. Zhang, Y. Zhou, J. Li, J. Li, S. Sun, *Angew. Chemie Int. Ed.* **2021**, 10.1002/anie.202112447.
- [24] J. Mei, T. Liao, G. A. G. A. Ayoko, J. Bell, Z. Sun, *Prog. Mater. Sci.* **2019**, *103*, 596.
- [25] K. Qian, Y. Yan, S. Xi, T. Wei, Y. Dai, X. Yan, H. Kobayashi, S. Wang, W. Liu, R. Li, *Small* **2021**, 2102970.
- [26] C. Wang, H. Shang, Y. Wang, H. Xu, J. Li, Y. Du, *J. Mater. Chem. A* **2021**, *9*, 14601.
- [27] L. Reith, C. A. Triana, F. Pazoki, M. Amiri, M. Nyman, G. R. Patzke, *J. Am. Chem. Soc.* **2021**, *143*, 15022.
- [28] H. Jiang, Q. He, X. Li, X. Su, Y. Zhang, S. Chen, S. Zhang, G. Zhang, J. Jiang, Y. Luo, P. M. Ajayan, L. Song, *Adv. Mater.* **2019**, *31*, 1805127.

- [29] N. Li, H. Tan, X. Ding, H. Duan, W. Hu, G. Li, Q. Ji, Y. Lu, Y. Wang, F. Hu, C. Wang, W. Cheng, Z. Sun, W. Yan, *Appl. Catal. B Environ.* **2020**, *266*, 118621.
- [30] J. X. Liu, H. Y. Su, D. P. Sun, B. Y. Zhang, W. X. Li, *J. Am. Chem. Soc.* **2013**, *135*, 16284.
- [31] X. Ma, A. M. Nolan, S. Zhang, J. Bai, W. Xu, L. Wu, Y. Mo, H. Chen, *J. Am. Chem. Soc.* **2018**, *140*, 17290.
- [32] A. N. Enyashin, L. Yadgarov, L. Houben, I. Popov, M. Weidenbach, R. Tenne, M. Bar-Sadan, G. Seifert, *J. Phys. Chem. C* **2011**, *115*, 24586.
- [33] Y. Chen, Z. Lai, X. Zhang, Z. Fan, Q. He, C. Tan, H. Zhang, *Nat. Rev. Chem.* **2020**, *4*, 243.
- [34] B. Zhang, L. Wang, Z. Cao, S. M. Kozlov, F. P. García de Arquer, C. T. Dinh, J. Li, Z. Wang, X. Zheng, L. Zhang, Y. Wen, O. Voznyy, R. Comin, P. De Luna, T. Regier, W. Bi, E. E. Alp, C. W. Pao, L. Zheng, Y. Hu, Y. Ji, Y. Li, Y. Zhang, L. Cavallo, H. Peng, E. H. Sargent, *Nat. Catal.* **2020**, *3*, 985.
- [35] V. H. Hoa, D. T. Tran, D. C. Nguyen, D. H. Kim, N. H. Kim, J. H. Lee, *Adv. Funct. Mater.* **2020**, *30*, 2002533.
- [36] B. Cao, G. M. Veith, J. C. Neufeind, R. R. Adzic, P. G. Khalifah, *J. Am. Chem. Soc.* **2013**, *135*, 19186.
- [37] H. Cheng, Q. Liu, Y. Diao, L. Wei, J. Chen, F. Wang, *Adv. Funct. Mater.* **2021**, *31*, 2103732.
- [38] J. Mei, T. Liao, H. Spratt, G. A. Ayoko, X. S. Zhao, Z. Sun, *Small Methods* **2019**, *3*, 1900055.
- [39] M. Yu, Z. Z. Wang, C. Hou, Z. Z. Wang, C. Liang, C. Zhao, Y. Tong, X. Lu, S. Yang, *Adv. Mater.* **2017**, *29*, 1602868.
- [40] X. Li, J. Wei, Q. Li, S. Zheng, Y. Xu, P. Du, C. Chen, J. Zhao, H. Xue, Q. Xu, H. Pang, *Adv. Funct. Mater.* **2018**, *28*, 1800886.
- [41] X. Wang, Z. Liao, Y. Fu, C. Neumann, A. Turchanin, G. Nam, E. Zschech, J. Cho, J. Zhang, X. Feng, *Energy Storage Mater.* **2020**, *26*, 157.
- [42] Y. Wang, C. Xie, Z. Zhang, D. Liu, R. Chen, S. Wang, *Adv. Funct. Mater.* **2018**, *28*, 1703363.
- [43] W. Chen, J. Huang, J. Wei, D. Zhou, J. Cai, Z. Da He, Y. X. Chen, *Electrochem. commun.* **2018**, *96*, 71.
- [44] D. A. Kuznetsov, B. Han, Y. Yu, R. R. Rao, J. Hwang, Y. Román-Leshkov, Y. Shao-Horn, *Joule* **2018**, *2*, 225.
- [45] C. Alex, S. C. Sarma, S. C. Peter, N. S. John, *ACS Appl. Energy Mater.* **2020**, *3*, 5439.
- [46] Z. Xiao, Y. C. Huang, C. L. Dong, C. Xie, Z. Liu, S. Du, W. Chen, D. Yan, L. Tao, Z. Shu, G. Zhang, H. Duan, Y. Wang, Y. Zou, R. Chen, S. Wang, *J. Am. Chem. Soc.* **2020**, *142*, 12087.
- [47] A. Bergmann, T. E. Jones, E. Martinez Moreno, D. Teschner, P. Chernev, M. Gliech, T. Reier, H. Dau, P. Strasser, *Nat. Catal.* **2018**, *1*, 711.
- [48] Z. Chen, C. X. Kronawitter, Y. W. Yeh, X. Yang, P. Zhao, N. Yao, B. E. Koel, *J. Mater. Chem. A* **2017**, *5*, 842.
- [49] J. Villalobos, D. González-Flores, R. Urcuyo, M. L. Montero, G. Schuck, P. Beyer, M. Risch, *Adv. Energy Mater.* **2021**, *11*, 2101737.
- [50] J. Li, S. Chen, N. Yang, M. Deng, S. Ibraheem, J. Deng, J. Li, L. Li, Z. Wei, *Angew. Chemie - Int. Ed.* **2019**, *58*, 7035.
- [51] J. Hwang, R. Walczak, M. Oschatz, N. V. Tarakina, B. V. K. J. Schmidt, *Small* **2019**, *15*, 1901986.
- [52] J. Abed, S. Ahmadi, L. Laverdure, A. Abdellah, C. P. O'Brien, K. Cole, P. Sobrinho, D. Sinton, D. Higgins, N. J. Mosey, S. J. Thorpe, E. H. Sargent, *Adv. Mater.* **2021**, 2103812.

- [53] A. Wu, Y. Xie, H. Ma, C. Tian, Y. Gu, H. Yan, X. Zhang, G. Yang, H. Fu, *Nano Energy* **2018**, *44*, 353.
- [54] B. S. Youmbi, F. Calvayrac, *Surf. Sci.* **2014**, *621*, 1.
- [55] B. C. Shih, T. A. Abteu, X. Yuan, W. Zhang, P. Zhang, *Phys. Rev. B* **2012**, *86*, 165124.

Table of Content

Title: Molybdenum-promoted Surface Reconstruction Kinetics in Polymorphic Cobalt for Initiating Rapid Oxygen Evolution

Authors: Juan Bai, Jun Mei* Ting Liao* Qiang Sun, Zhi-Gang Chen, Ziqi Sun*

Ultrathin two-dimensional (2D) polymorphic cobalt nanosheets structure is proposed to modulate surface reconstruction kinetics for alkaline OER. By structural tracking on the initial surface reconstruction stage via XPS technique, it is concluded that the presence of molybdenum is beneficial to promoting the desired phase transition and stabilizing real reaction sites.

